

A new electron-multiplier-tube-based beam monitor for muon monitoring at the T2K experiment

Y. Ashida^{a,*}, M. Friend^b, A. K. Ichikawa^a, T. Ishida^b, H. Kubo^a,
K. G. Nakamura^a, K. Sakashita^b, W. Uno^a

^a*Department of Physics, Kyoto University, Kyoto 606-8502, Japan*

^b*High Energy Accelerator Research Organization (KEK), Tsukuba, Ibaraki, Japan*

Abstract

A muon beam monitor is an indispensable component for accelerator-based long baseline neutrino oscillation experiments to monitor and control the neutrino beam. Though Si photodiodes and ionization chambers have been successfully used as muon monitors at the T2K experiment, more radiation tolerant sensors are desired for the future operation. Electron-multiplier tubes (EMTs) are one candidate. Secondary electrons produced by the passage of muons at dynodes are multiplied in the tube and produce signal. Two prototype detectors were installed at the T2K muon monitor location, and several EMT properties were studied based on data with the T2K muon beam. The signal size is as expected based on calculation. The EMTs show sufficiently fast time response for bunch-by-bunch beam monitoring. The spill-by-spill intensity resolution is 0.4% and better than the required value (1%). Signal linearity within $\pm 1\%$ is achieved up to 500 kW with +250 kA horn operation. A gradual signal decrease is observed during the initial exposure due to stabilization of dynode materials before the response becomes stable within $\pm 1\%$. This work demonstrates that EMTs may be useful for future muon monitoring.

1. Introduction

The importance of beam monitoring is growing both to protect equipment in high intensity beam facilities and to precisely measure beam properties. The beam intensity can span many orders of magnitude, from one to 10^{14} particles per pulse. Counting detectors are applicable when the intensity is up to order $10^7/s$, but do not work at higher intensity. Current-mode read-out is used in such cases. When the number of charged particles exceeds around $10^{15}/s$, a secondary emission monitor, the signal of which is an electrical current induced by the emission of secondary electrons from a conductor foil by radiation, has sufficiently large signal for 50- Ω -load read-out. For intermediate intensities still too high for particle counting, detectors utilizing ionization or excitation of media, such as semi-conductors, scintillators, and gases, are used.

For accelerator neutrino beam experiments, monitoring the muons produced along with neutrinos has played a key role in beam control (See [1, 2] and references therein). Ionization

*Corresponding author

Email address: assy@scphys.kyoto-u.ac.jp (Y. Ashida)

detectors and Si photodiodes have been used at the T2K experiment, when the typical number of muons is $10^{12}/\text{s}$. However, during the recent high intensity operation, as is described later, radiation damage of Si sensors and signal saturation of ionization detectors start to become issues.

In this paper, we report the investigation of electron-multiplier tubes, or EMTs, equivalently, photomultiplier tubes (PMTs) without a photocathode, as a new muon monitor for the T2K experiment. After a description of the T2K muon monitor and its situation in Section 2, we describe the principle of muon monitoring using electron-multiplier tubes in Section 3 and our EMT prototype sensors in Section 4. Then, we report the initial performance test results obtained with the muon beam at the T2K muon monitor location in Section 5 before the conclusion in Section 6.

2. The muon monitor for the T2K experiment

2.1. The T2K experiment and J-PARC neutrino beamline

The T2K experiment measures neutrino oscillation parameters precisely using accelerator produced (anti-)neutrinos [3]. A muon neutrino or anti-neutrino beam is produced at Japan Proton Accelerator Research Complex (J-PARC) and then measured at the Super-Kamiokande (SK) detector [4] which is located 295 km away. By measuring the disappearance of muon (anti-)neutrinos and the appearance of electron (anti-)neutrinos, T2K determines neutrino oscillation parameters and probes CP-violation in the lepton sector [5, 6].

A 30 GeV proton beam from the Main Ring (MR) synchrotron of J-PARC impinges on a graphite target to produce predominantly pions and some fraction of kaons. Among those particles, either positively or negatively charged particles are parallel-focused by three magnetic horns [7, 8], currently operated at positive or negative 250 kA. The hadrons then decay into neutrinos and muons in a 96-m-long decay volume, producing a neutrino beam or an anti-neutrino beam, respectively. Both the direction and intensity of the neutrino beam must be known precisely in order to precisely predict the neutrino flux at SK. The neutrino beam profile spreads as wide as a few km at SK, but a 1 mrad change in the direction of the beam axis causes a significant change in the event rate and a distortion of the energy spectrum, which leads to large systematic errors on the neutrino flux. Near detectors sit 280 m downstream of the target to monitor the beam direction and intensity, as well as to study neutrino-nucleus interactions. One of the near detectors, INGRID, is composed of 14 modules arranged in a cross spanning $10\text{ m} \times 10\text{ m}$ around the beam center axis and monitors the beam direction and intensity by measuring the event rate at each module [9]. The INGRID gives direct information about the neutrino beam properties, however, it requires more than one day to accumulate sufficient data for a neutrino beam profile measurement because of the quite small interaction cross section of neutrinos. On the other hand, as explained below, the muon monitor can reconstruct the beam profile for each beam bunch.

The neutrino beam direction is affected by various sources, i.e. the position of the proton beam at the target, mis-alignment of the target or horns, etc. In each 2.48-second beam cycle, a proton beam spill composed of 8 bunches, typically having 30 ns full-width-half-maximum (FWHM) and separated by 581 ns, is extracted to the neutrino beamline. Bunch-by-bunch beam monitoring is indispensable for primary proton beam tuning and diagnostics of the proton beam and beamline equipment. The proton beam intensity is monitored by five Current Transformers (CT), and the position and profile of the proton beam are measured by

nineteen Segmented Secondary Emission Monitors (SSEM). In this paper, we use the values measured by the most downstream monitors, CT5, SSEM18, and SSEM19. Though there is an Optical Transition Radiation monitor (OTR) [10] nearest the target, its information is not used here because it usually doesn't give precise information at low intensities, where the beam studies often have been conducted, because of operational trouble which occurred in 2015. In addition to the proton beam monitors, T2K has a muon monitor which monitors the profile and intensity of the muons produced along with the neutrinos. They sit 118 m away from the target, downstream of a beam dump, at the end of T2K decay volume. The target, horns, and part of the beam dump which is made of graphite blocks are in a vessel filled with helium gas. A second part of the beam dump is downstream of the He vessel and is composed of concrete blocks. This is followed by the muon monitor which also sits outside the helium vessel. The beam dump thickness is designed such that only muons with momentum higher than 5 GeV penetrate it, while hadrons and low-momentum muons are absorbed. While the proton monitors directly monitor the proton beam properties, the muon monitor measurement is more correlated with the neutrino beam itself. These monitors give bunch-by-bunch information and have been used for proton beam tuning and alignment check of the target, horns, and baffle located upstream the target. Figure 1 shows a schematic drawing of the beamline equipment from the most downstream part of the primary beamline to the muon monitor.

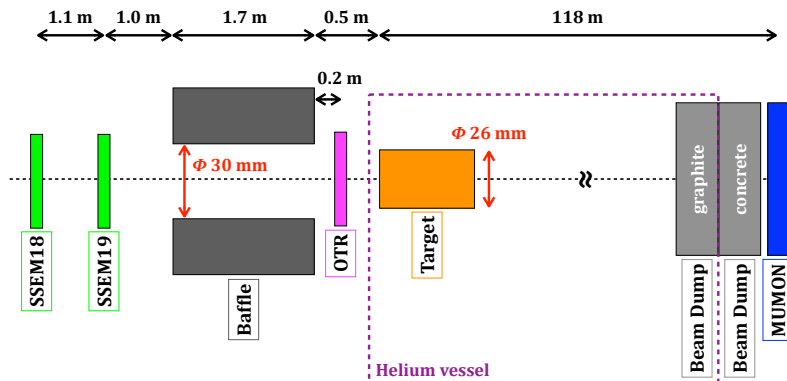


Figure 1: Schematic drawing of the beamline equipment from the most downstream part of the neutrino primary beamline to the muon monitor.

2.2. The muon monitor (MUMON)

The current muon monitor (MUMON) system is composed of two arrays of sensors, one of silicon PIN photodiodes (Si; HAMAMATSU[®] S3590-08) and another of ion chambers (IC; Ar+N₂ or He+N₂) [11], where the Si array sits upstream of the IC array. Each array covers a 150 × 150 cm² region with 7 × 7 channels installed with a 25 cm pitch. A schematic view of the MUMON is shown in Figure 2. Seventy-m-long polyimide cables for signal and high-voltage are drawn from the underground muon monitor location to an electronics hut on the ground. The sensor waveforms are stored with 65 MHz sampling by “COPPER” (KEK-made Flash-ADC modules) [12]. At high intensity beam operation, additional attenuation modules are used to attenuate the signal size to be within the Flash-ADC dynamic range. The precision

of the MUMON beam center measurement is 0.28 mrad and the resolution is better than 0.03 mrad [13]. During the beam operation, the MUMON continuously monitors the muon beam profile and intensity, and if any major deviation from the expected muon beam profile is measured an alarm is issued and the proton beam is tuned. The system has been working well since the beginning of the T2K experiment. When the horn current is set to +250 kA (neutrino beam mode), the muon flux at the MUMON is 1.09×10^5 /cm²/10¹² POT (protons on target). At 485 kW proton beam power (current maximum power), the muon flux is 3.45×10^6 /cm²/bunch. For -250 kA (anti-neutrino beam mode), the muon flux becomes about two thirds of that at +250 kA due to the difference in the focused pion flux.

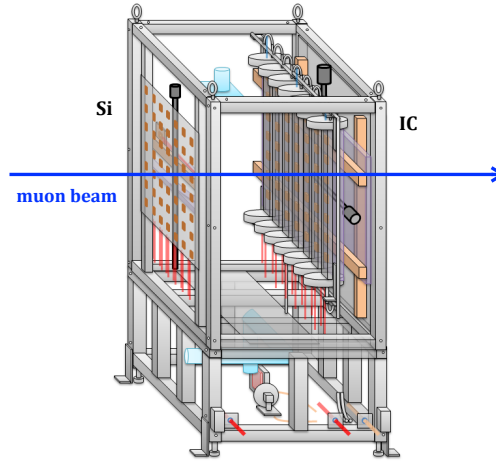


Figure 2: Schematic view of the T2K muon monitor [11]. Each array of Si and IC sensors covers a 150×150 cm² region with 7×7 channels.

2.3. Concerns for the current muon monitors

There is a plan to increase the J-PARC beam power up to 1.3 MW from 485 kW and the horn current to 320 kA from 250 kA [14]. In this situation, the muon flux is expected to become about three times larger than the current flux. For instance, the muon flux at 1.3 MW and +320 kA is 1.02×10^7 /cm²/bunch (1.75×10^{14} /cm²/s). Under such a large muon flux irradiation, we expect certain issues with the current muon monitors, some of which are already observed even at the present muon flux.

The Si sensors will suffer radiation damage, and monthly regular replacements will be necessary. Figure 3 shows the evolution of the ratio of the total yield of the Si and IC (Ar gas) sensors over several J-PARC operation periods. By taking the ratio of two, fluctuations from other sources such as the proton beam condition or horn current are canceled. The ratio has decreased by 1.2% after irradiation of about 7×10^{20} POT at +250 kA horn current. The fact that the IC yield was stable within $\pm 0.2\%$ during that period indicates that the Si sensors themselves show signal degradation due to radiation damage.

For the ion chambers, non-linear signal response due to space charge effects becomes an issue at high intensity. When many electrons and ions are generated, the electric field is distorted by accumulated ions, which affects the signal yield. This effect appears more severely at latter bunches because more ions are accumulated. The left panel of Figure 4 shows the

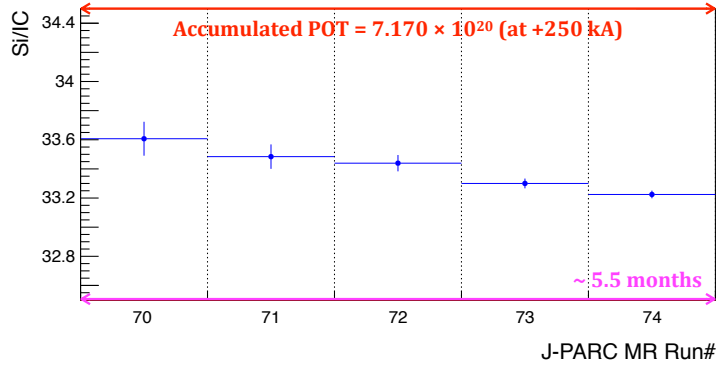


Figure 3: Si and IC (Ar) yield average ratio over several MR runs all with horn current of +250 kA. A 1.2% decrease is seen after an accumulated POT of 7×10^{20} .

IC (Ar) yield for the 8th bunch at various beam powers (all at +250 kA horn current), and indicates non-linearities appear at 400 kW. The right panel shows the IC yield divided by the Si yield for each bunch, and a drop in the ratio is clearly seen for the final bunch. Here, the beam power and horn current are 460 kW and +250 kA, respectively. There can be three solutions to this problem. One is to increase the applied high-voltage so that generated ions are swept faster, however, there is a risk of reaching breakdown voltage. Another solution is to use a lighter gas, such as He, in which the number of electron and ion pairs is much smaller than Ar, and therefore less charge accumulation is achieved. However, lighter gases can suffer from signal pileup caused by the fast drift speed of lighter ions, as shown in Figure 5 for He. This affects the bunch-by-bunch monitoring. Another lighter noble gas under consideration is Ne, however, Ne gas is quite expensive now. Usage of a thinner gap between the electrodes could be a solution, but this would require a full replacement of the current T2K IC system.

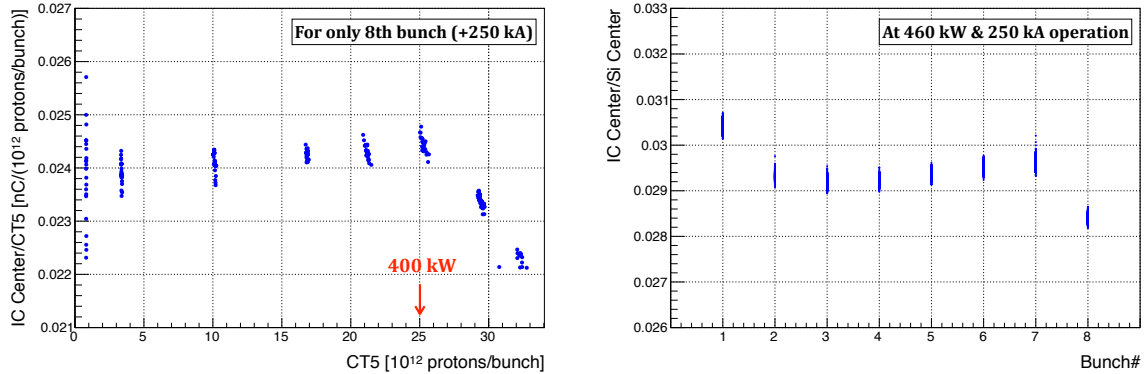


Figure 4: IC yield for the 8th bunch at various beam powers at +250 kA horn current (left) and the ratio of IC yield to Si yield for each bunch at 460 kW and +250 kA horn current operation (right). The features seen in bunches 1~7 can be understood by the signal tail properties: the Si sensors have larger and shorter tails than the IC, as shown in Figure 11. The decrease in the 8th bunch is due to space charge effects in the IC.

For these reasons, a new T2K muon monitoring system is desired for the future. Electron-multiplier tubes (EMTs) are one candidate, as described below.

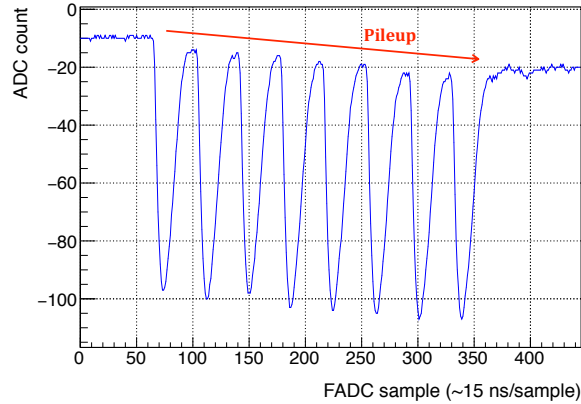


Figure 5: An example of the IC signal waveform when He gas is used. The beam power and horn current settings are 340 kW and +250 kA, respectively.

3. Beam monitoring by electron-multiplier tubes

High radiation resistance is required for the new detector. Fast signal response is also required to monitor the beam on a bunch-by-bunch basis. The secondary electron emission process is often used for high intensity beam monitoring at accelerators. In fact, the particle flux at the T2K primary beamline secondary emission monitors is much higher than that at the T2K muon monitor. Photomultiplier tubes (PMTs) use the secondary emission process to multiply the electron signal from the PMT photocathode. Secondary emission electrons are also produced by the passage of muons, and their signal can also be multiplied in a PMT. For muon monitoring, however, the photocathode is not necessary. An electron-multiplier tube (EMT), a PMT without a photocathode, is considered as a candidate for the new muon monitor. In our study, EMTs are produced by depositing aluminum on the cathode of PMTs. Figure 6 shows a schematic diagram of the signal multiplication of an EMT.

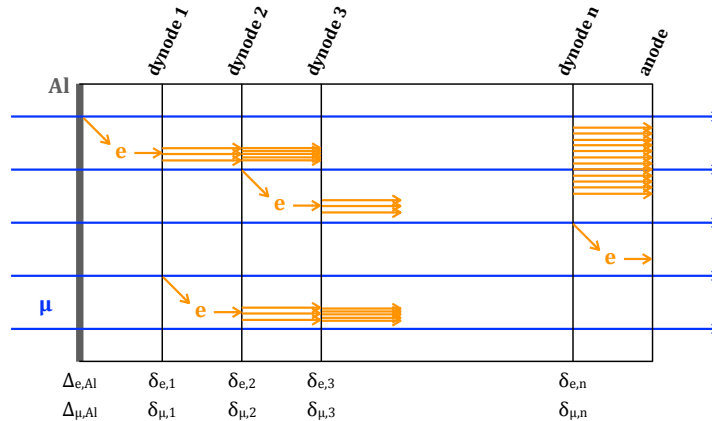


Figure 6: Schematic diagram of the signal multiplication by an electron-multiplier tube as a muon monitor. Secondary emissions by electrons and muons occur at each dynode and at the Al surface.

When a muon passes through the EMT, secondary electrons are produced either at the surrounding aluminum cathode or the dynodes. The emitted electrons are accelerated, bombard the downstream dynodes, and produce more electrons. The secondary emission efficiency is defined as the number of emitted electrons divided by the number of incident particles [15]. It is a characteristic of the material type, the incident particle type, and the particle energy. In Figure 6, Δ represents the secondary emission efficiency for aluminum and δ is that for dynodes. To specify the incident particle, an “ e ” subscript is used for electrons and a “ μ ” is used for muons. The numbers subscript for δ corresponds to the dynode number. The product of the secondary emission efficiency of all dynodes determines the gain of the PMT:

$$G = \delta_{e,1} \times \delta_{e,2} \times \cdots \times \delta_{e,n} = \prod_{i=0}^n \delta_{e,i}. \quad (1)$$

In the case of the muon monitor, the signal is generated primarily by muons and electrons (delta-rays) knocked-out by muons. The energy of the delta-rays reaches up to several hundred MeV [13]. These muons and delta-rays penetrate the EMT, while most of the secondary emission electrons stop once they hit the dynodes. Therefore, it is possible that secondary electrons which contribute to the signal are produced at every dynode by muons or delta-rays. The final output signal Q can be written as follows:

$$Q = Q_\mu + Q_e, \quad (2)$$

$$Q_\mu = e \cdot \phi_\mu \cdot \left\{ A_{\text{sur}} \cdot \Delta_{\mu,\text{Al}} \cdot \prod_{i=1}^n \delta_{e,i} + \sum_{i=1}^{n-1} \left(A_i \cdot \delta_{\mu,i} \cdot \prod_{j=i+1}^n \delta_{e,j} \right) \right\}, \quad (3)$$

$$Q_e = e \cdot \phi_e \cdot \left\{ A_{\text{sur}} \cdot \Delta_{e,\text{Al}} \cdot \prod_{i=1}^n \delta_{e,i} + \sum_{i=1}^{n-1} \left(A_i \cdot \delta_{e,i} \cdot \prod_{j=i+1}^n \delta_{e,j} \right) \right\}, \quad (4)$$

where e is the elementary electric charge (1.6×10^{-19} C), A_{sur} and A_i are the sensitive area of the aluminum cathode surface and each dynode surface [cm^2], respectively, and ϕ_μ (ϕ_e) is the muon (delta-ray) flux [$/\text{cm}^2$]. The first term corresponds to the secondary electron production at the aluminum cathode, and the second term to that at the i -th dynode.

As a simple case for a rough estimation, the contribution from delta-rays is ignored here and the sensitive areas of the Al and dynodes’ surfaces are all assumed to be A . Here we assume that particles are incident on the EMT perpendicular to the surface and any change of the dynode effective surface area is not considered. In addition, the electron secondary emission efficiencies of all dynodes ($\delta_{e,i}$) are assumed to be the same (referred to as δ_e , hereafter). The typical gain of HAMAMATSU[®] R9880, which is used for the EMT, is 5×10^3 when -500 V is applied, and the number of dynodes is $n = 10$. Therefore, the gain per dynode can be calculated as $\delta_e \sim 2.35$. The secondary emission efficiencies for muons with several GeV energy, $\Delta_{\mu,\text{Al}}$ and $\delta_{\mu,i}$, are assumed to be 0.08 [16]. The sensitive area is $A = 2.01 \text{ cm}^2$ (radius is 8 mm), and the normalized muon flux at horn current $+250$ kA is $\phi_\mu^{\text{normalized}} = 1.09 \times 10^5 / \text{cm}^2 / 10^{12}$ POT. Using the number of protons at beam power 460 kW, $N = 3.0 \times 10^{13}$ POT/bunch, the muon flux is calculated as $\phi_\mu = \phi_\mu^{\text{normalized}} \cdot N$. With these assumptions, the expected charge is calculated as 730 pC/bunch.

4. Prototype detectors

Two EMTs were specially made based on the HAMAMATSU[®] metal-package PMT R9880 by depositing aluminum on the cathode. Figure 7 shows a schematic diagram of the divider circuit used to operate these EMTs. The resistances $R_1 \sim R_{10}$ are set to 330 k Ω , and R_{11} is set to 160 k Ω , giving uniform voltage differences between the dynodes. The maximum negative high voltage applied to the cathode is limited to -500 V due to the currently-installed connectors in the T2K muon monitor system. The capacitors, $C_1 \sim C_{11}$, compensate for the charge consumed on the dynodes in the process of multiplication. To keep linearity in the EMT response, sufficient charge, usually 100 \sim 1000 times than the consumed charge, has to be stored in these capacitors [15]. The 51 Ω damping resistances, R_{12} and R_{13} , are usually inserted to reduce waveform ringing, but we removed them so that the charge consumed in earlier bunches is quickly compensated for from the capacitors.

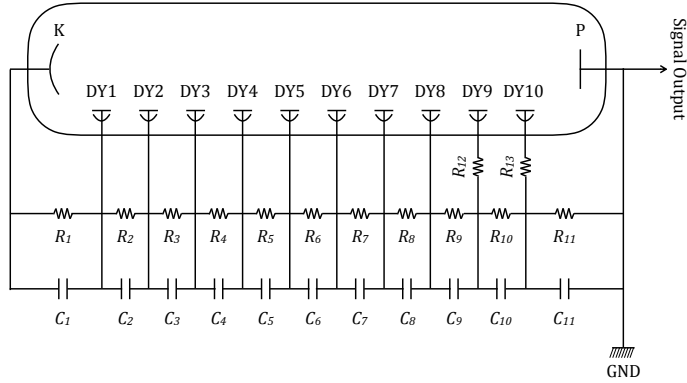


Figure 7: Schematic diagram of the divider circuit of the prototype EMT. “K”, “P”, “DY” and “GND” represent the cathode, anode, dynode, and ground, respectively. The resistances $R_1 \sim R_{10}$ are 330 k Ω , and R_{11} is 160 k Ω . The capacitances are given in Table 1.

We made four sets of divider circuits. The capacitances of the later versions were optimized based on the initial measurement results with the earlier versions. In this paper, results of measurements with the later two versions, referred to as EMTC3 and EMTC4, are reported. Table 1 summarizes the capacitances and stored charges of each capacitance used in EMTC3 and EMTC4 when a negative bias of -500 V is applied. Only C_8 to C_{11} for EMTC3 and C_6 to C_{11} for EMTC4 are used and other capacitances were removed (represented as “-” in Table 1). Figure 8 shows a photograph of EMTC3 and its divider circuit.

The EMTs C3 and C4 were installed just downstream of the T2K MUMON ion chamber. Figure 9 indicates the installation position in the left panel and shows an actual photograph in the right panel. The EMT sensors are located centered vertically and 26.5 cm away from the MUMON center horizontally. The signal and high-voltage cables are the same as those used for the Si and IC sensors. The read-out system is also the same, however, the attenuator module is not used for the EMTs.

Table 1: Capacitances and stored charges for the EMTs when -500 V is applied.

	EMTC3		EMTC4	
	capacitance (nF)	charge (μC)	capacitance (nF)	charge (μC)
K-DY1 (C_1)	-	-	-	-
DY1-2 (C_2)	-	-	-	-
DY2-3 (C_3)	-	-	-	-
DY3-4 (C_4)	-	-	-	-
DY4-5 (C_5)	-	-	-	-
DY5-6 (C_6)	-	-	100	4.8
DY6-7 (C_7)	-	-	100	4.8
DY7-8 (C_8)	10	0.48	100	4.8
DY8-9 (C_9)	10	0.48	330	15.7
DY9-10 (C_{10})	10	0.48	330	15.7
DY10-GND (C_{11})	15	0.35	330	7.6

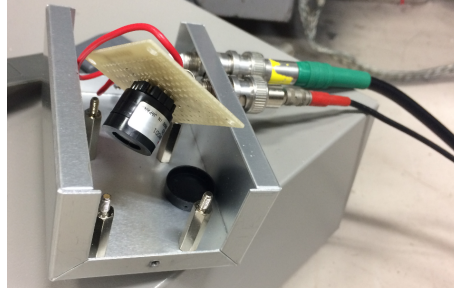


Figure 8: A photograph of EMTC3 and its divider circuit.

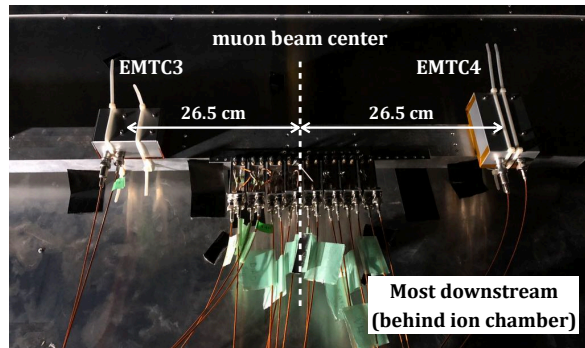
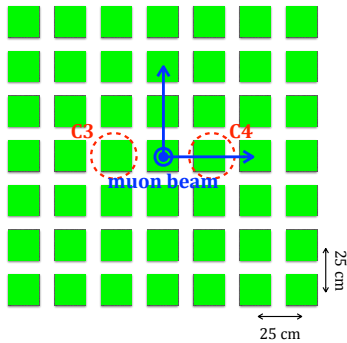


Figure 9: Prototype EMTs' horizontal and vertical installation positions overlaid with the IC sensor positions (left) and a photograph of the installed detectors (right). Green squares in the left figure indicate the 49 channels of the ion chamber.

5. Muon beam test

The performance of the EMTs (C3 and C4), including checks of the signal size, time response, intensity resolution, linearity, and stability, were studied using the T2K muon beam.

5.1. Output charge

The expected output charge of an EMT was calculated in Section 3 as 730 pC/bunch at 460 kW beam power and +250 kA horn current. The measured charge output from each bunch for the EMTC3 and C4, when -500 V is applied, is summarized in Table 2. Reasonable agreement with our expectation is seen.

Table 2: EMT output signal size per bunch at 460 kW beam intensity and +250 kA horn current with applied voltage of -500 V. The expected charge is 730 pC/bunch.

Bunch#	EMTC3 charge [pC]	EMTC4 charge [pC]
1	873.1	784.9
2	870.7	787.3
3	866.9	788.6
4	855.9	787.9
5	860.4	797.0
6	850.6	795.5
7	847.8	798.5
8	854.1	797.7
Average	859.9	792.2

5.2. Signal waveform

Figure 10 shows examples of the EMTC3 (left panel) and C4 (right panel) signal waveform. The signal has a tail component caused by both detector intrinsic properties and cable and electronics reflections. Such tails could deteriorate bunch-by-bunch monitoring. To quantify the tail contribution, we calculate the ratio of the integral of the tail region to that of the 1st bunch signal for the EMTs, the Si center sensor, and the IC center sensor. Two different integration regions, Tail-1 and Tail-2 shown in Figure 10, are selected with the same sampling period as the one used for integrating the signal in bunch 1. The tail sizes are shown in Figure 11. It can be seen that EMTs have a smaller tail component (about 1%) than the Si or IC sensors (few %), and the tail is also short.

5.3. Intensity resolution

Figure 12 shows the spill-by-spill detector signal size normalized to the proton beam intensity for the EMTs, Si center channel, and IC (Ar) center channel at a proton beam power of 450 kW and horn current of +250 kA. From these distributions, the EMT intensity resolution is calculated to be 0.34% for C3 and 0.41% for C4, while the Si and IC (Ar gas) center channels show 0.25% and 0.24% resolutions, respectively. The resolutions of each detector are summarized in Table 3, including the intensity resolution for only the 1st bunch. The statistical error on each value is quite small (less than 0.01%). The contribution from noise due to the read-out system including the cable, attenuator, and Flash-ADC is estimated

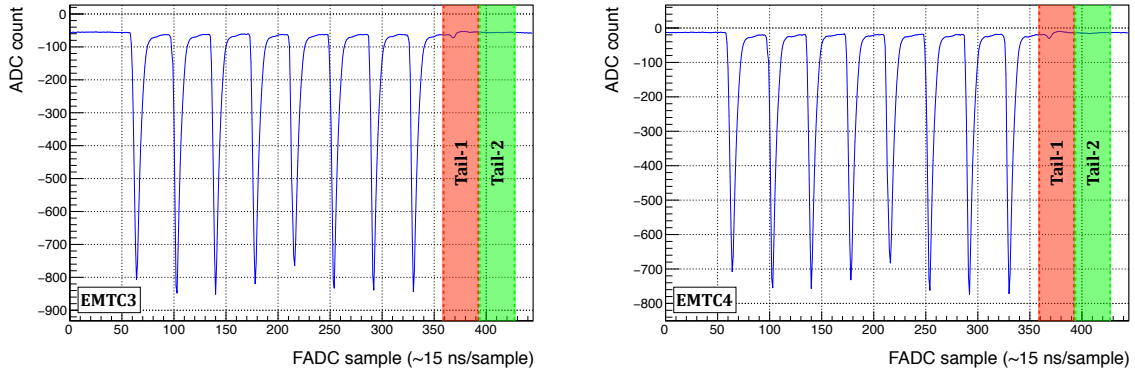


Figure 10: EMTC3 (left) and C4 (right) waveform examples. Two tail regions, Tail-1 and Tail-2, are selected to estimate the tail component contribution.

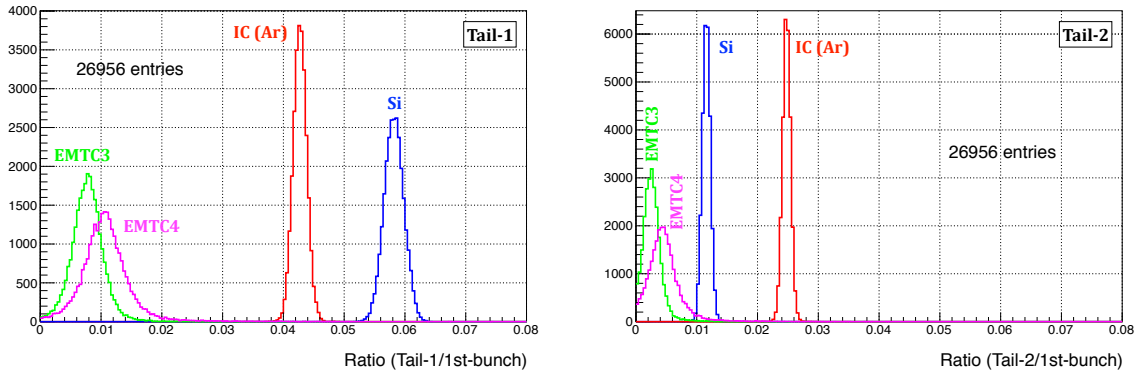


Figure 11: Tail sizes for Tail-1 (left) and Tail-2 (right). The tail integration regions are shown in Figure 10. The EMTs show a smaller tail component than the Si and IC (Ar) sensors. Si has a larger but faster tail than IC (Ar).

by integrating the baseline before the beam spill and is found to be less than 0.1%. Compared to the current monitors EMTs show slightly poor resolution, however, it is not an issue for the following reason. The 1% uncertainty of the intensity measurement for each sensor corresponds to an 0.06 mrad uncertainty in the beam direction measurement, which is much smaller than the total precision of 0.28 mrad. In fact, the total intensity monitoring precision is limited by the calibration of the read-out system, the precision of which is a few %. In conclusion, the intensity resolution of the EMTs satisfies the requirements for muon beam direction and flux measurements.

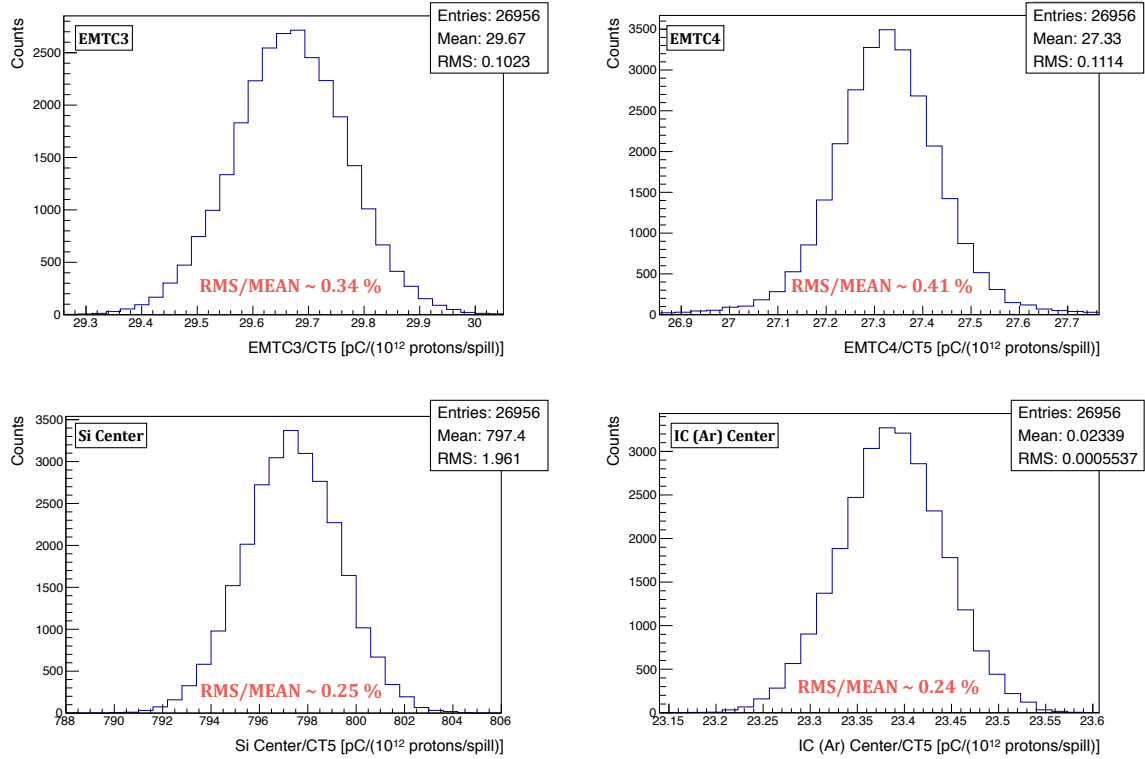


Figure 12: The normalized signal size of EMTC3 (left top), C4 (right top), Si center (left bottom), and IC (Ar) center (right bottom) at 450 kW beam power and +250 kA horn current. C3 shows 0.34%, C4 0.41%, Si 0.25%, and IC 0.24% intensity resolution.

Table 3: Summary of the intensity resolution of each detector for spill-by-spill and first bunch measurements. The proton beam intensity is 450 kW and the horn current setting is +250 kA. Statistical uncertainty is less than 0.01%.

Detector	Spill (8 bunch sum)	First bunch
EMTC3	0.34%	0.73%
EMTC4	0.41%	0.78%
Si center	0.25%	0.37%
IC (Ar) center	0.24%	0.33%

5.4. Linearity

A linear sensor response is desired to correctly monitor the beam at low power during beam tuning up to high power during physics operation. In order to test the linearity performance of the EMTs, beam intensity scans were carried out. During scans, the proton beam power was set to 13 kW, 50 kW, 150 kW, 260 kW, 340 kW, 400 kW, 460 kW, and 500 kW, and the horn current setting was +250 kA. Two different voltages were applied to the EMTs to study space charge effects, which is caused when the number of produced electrons is so large that the electric field is significantly distorted and then signal yield is decreased similar to the IC case described in Section 2. We applied -450 V to reduce the number of secondary electrons, and compared the linearity performance to the -500 -V-applied-case. The scan conditions are summarized in Table 4.

Table 4: Beam powers and voltages used for beam intensity scans. Note that the ratio of the number of protons to the beam power at repetition rate of 2.48 sec is 5.3×10^{11} protons/spill/kW.

Scan	Beam power [kW]	Applied HV [V]
I	150, 260, 340, 400, 460	-500
II	260, 340, 400, 460	-450
III	13, 50	$-500, -450$
IV	500	-500

Since the muon yield is correlated with the horn current, a correction to the calculated yield is applied using a horn current monitor information. The correction factor is determined based on horn current scan results (See Ref. [13] for details about the correction). During the intensity scans, the proton beam position was kept within ± 0.5 cm, monitored by SSEM19 and 18, and the effect on the muon flux by this fluctuation is less than 1%. Therefore, no correction is needed for this. The proton beam width changes depending on the beam power, and this does affect the muon flux. A Monte Carlo (MC) simulation [17] was conducted to estimate the change of the muon flux at the EMT position for various values of the beam width, and the result is shown in Figure 14. This result is used for a yield correction. The beam width values are taken from SSEM18 since there were several unreliable points in the SSEM19 data during the beam intensity scan. The consistency between SSEM19 and 18 have been confirmed by other, reliable, points. To check the width correction validity, two different beam widths were used at the 150 kW point ($\sim 80 \times 10^{12}$ protons/spill) in Scan I.

Figure 15 shows the scan results for the Si center channel. Here, Si is selected because IC shows non-linearity as described in Section 2. The plot in the left panel shows the result before the beam width correction, and the plot in the right panel shows that after the correction. The horn current correction is applied for both. At low intensity, points are more scattered due to a poor signal-to-noise ratio because of the small signal size. Therefore, the linearity at scan points above 100 kW ($\sim 50 \times 10^{12}$ protons/spill) is considered more reliable. It is found that the beam width correction works very well, especially for the 150 kW points ($\sim 80 \times 10^{12}$ protons/spill) in Scan I, where, before the MC correction the distributions are separated due to the different beam widths. The linearity is kept within $\pm 1\%$ from 100 kW to 500 kW.

The linearity results for EMTC3 and C4 are shown in Figure 16 and 17, respectively. The results use both horn current and proton beam width corrections. The plots in the left panels

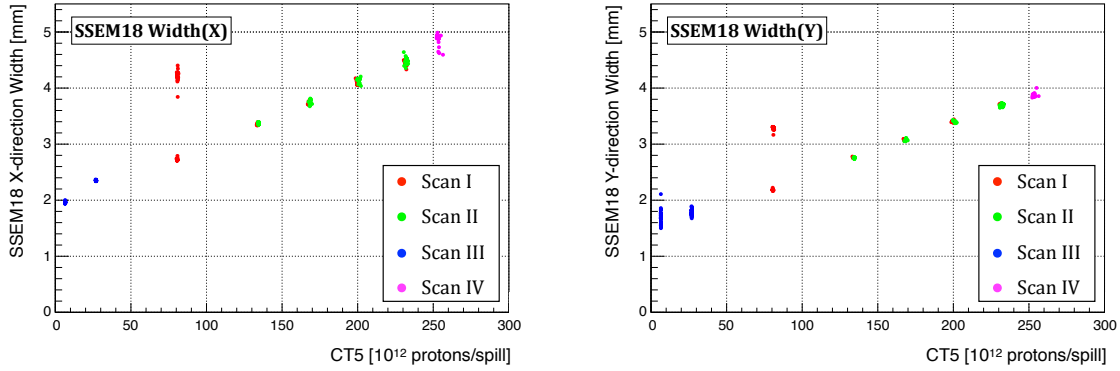


Figure 13: Proton beam width measured by SSEM18 during the beam intensity scans. The left (right) panel shows the results for X (Y). Different colors refer to different scans.

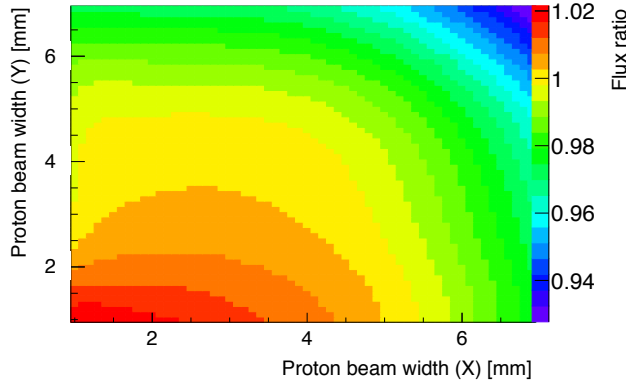


Figure 14: Ratio of the muon flux at the EMT position for various proton beam widths to the muon flux for beam width = (4, 4) mm.

show the results with -500 V high-voltage (HV) applied, while those in the right panels show the results with -450 V. EMTC4 shows better linearity performance than EMTC3, because the capacitance used in the circuit for C4 was improved as explained in Section 4. Measurements with lower voltage applied show better linearity, and this indicates that space charge effects exist when a higher voltage is applied. EMTC4 with -450 V shows as good linearity as the Si sensor up to 460 kW. At higher intensities, non-linearities may appear. To further improve linearity, use of a different dynode divider ratio can be considered, with a possible compromise of signal size.

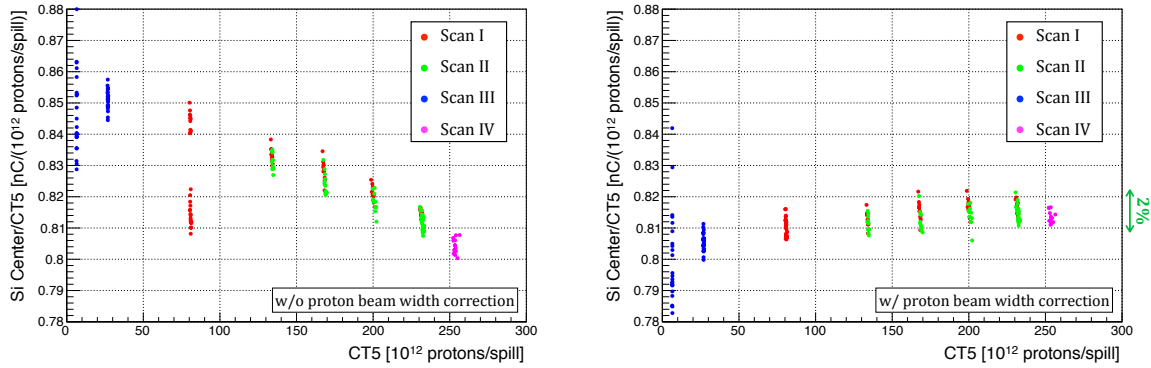


Figure 15: Results of the beam intensity scan for the Si center channel before (left) and after the proton beam width correction (right). Different colors correspond to different scans.

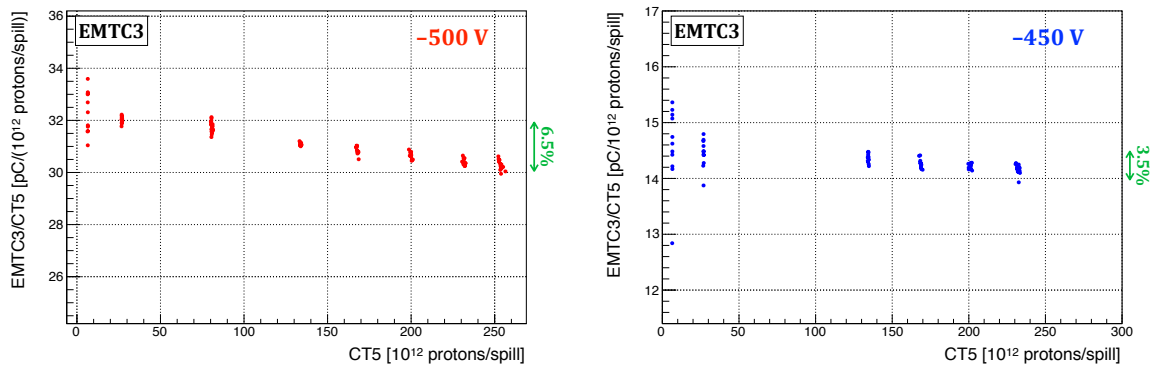


Figure 16: Results of the beam intensity scan for EMTC3. The left panel shows the result with -500 V high-voltage applied, and the right panel shows the result with -450 V applied.

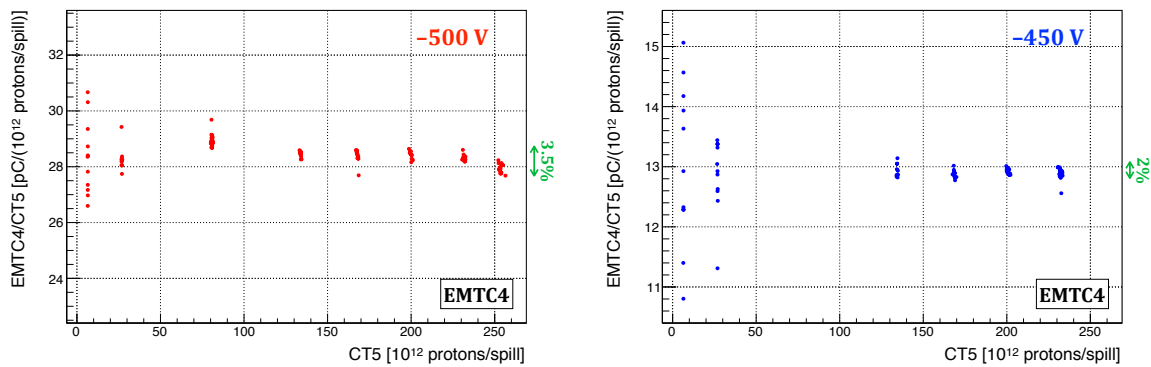


Figure 17: Results of the beam intensity scan for EMTC4. The left panel shows the result with -500 V high-voltage applied, and the right panel shows the result with -450 V applied.

5.5. Stability

The EMTs were continuously exposed to the T2K muon beam over five data taking periods. The beam conditions and applied HVs for each period are summarized in Table 5. Periods I and II are separated because EMTC4 was installed between them. EMTC3 was installed before Period I, when several trials, such as HV and attenuation level tuning, were performed. Therefore, the EMTC3 stability during the period before Period I is not shown here. There is an approximately half-year beam-off period between Period II and III, during which the EMTs’ HVs were turned off. Other than that, we turned off the HV of both EMTs for just one day in the middle of Period V in order to check the stability.

Table 5: Beam conditions and HVs for EMTC3 and C4 over beam exposures.

Period	Horn current [kA]	HV [V]	POT [$\times 10^{18}$]
I (23, Feb., 2017 \sim 30, Mar., 2017)	+250	−500	224.1
II (31, Mar., 2017 \sim 12, Apr., 2017)	+250	−500	76.8
III (16, Oct., 2017 \sim 22, Oct., 2017)	+250	−505	20.5
IV (22, Oct., 2017 \sim 2, Nov., 2017)	−250	−505	59.4
V (2, Nov., 2017 \sim 22, Dec., 2017)	−250	−450	305.8

Figures 18, 19, 20 and 21 show the yield vs. time for the Si center sensor, IC center sensor, EMTC3 and EMTC4, respectively. Effects of horn current to the muon flux are corrected as described in Subsection 5.4. There are two jumps seen in the EMTC3 signal, reason of which is still unknown, however, these seem to be synchronized with IC calibration work. Both EMTC3 and C4 show a drift in yield just after HV is first applied, in Periods I and III for C3, and Periods II and III for C4. This drift is considered to be due to the stabilization of the dynode materials, which are generally alkali metals and antimony (Sb). Usually PMTs require “warming-up” by irradiating with light for initial stabilization [15], however, EMTs cannot be warmed-up because they don’t have a photocathode. The required warm-up output charge is several μA for several minutes, which is equivalent to several mC. Table 6 shows the integrated charge output by the time the EMT signal yield became stable. The values are reasonable compared with the expected PMT warm-up charge. For later runs, both EMTC3 and C4 were stabilized after fewer POT. This is thought to be due to stabilization of the dynode materials at some level by the previous irradiation. After the drift period, the yield is basically stable within $\pm 1\%$, which is better than the accuracy of the read-out system calibration.

Table 6: Integrated charge output by the time the signal yield of each EMT became stable. The calculations for Period III use 1.1 times larger charge per bunch, since the applied HV is higher (−505 V). The recommended value for stabilization is several mC.

EMT number	Period	POT amount [$\times 10^{18}$]	Integrated charge [mC]
C3	I	~ 70	~ 2.0
	III	~ 13	~ 0.4
C4	II	~ 50	~ 1.3
	III	~ 13	~ 0.4

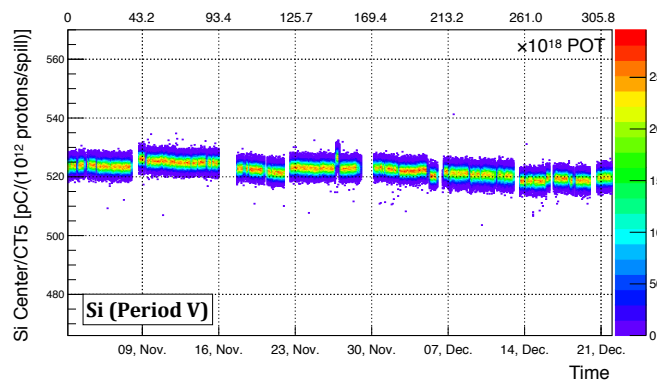
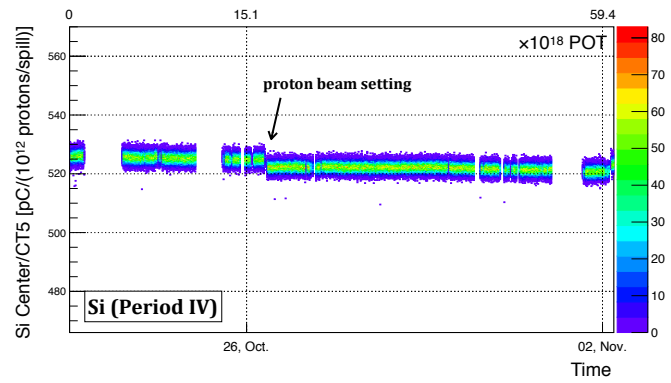
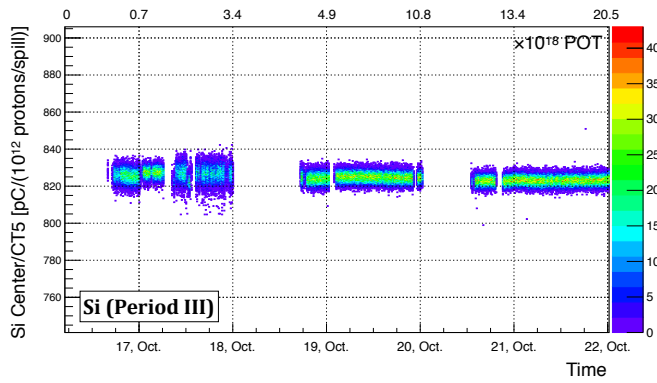
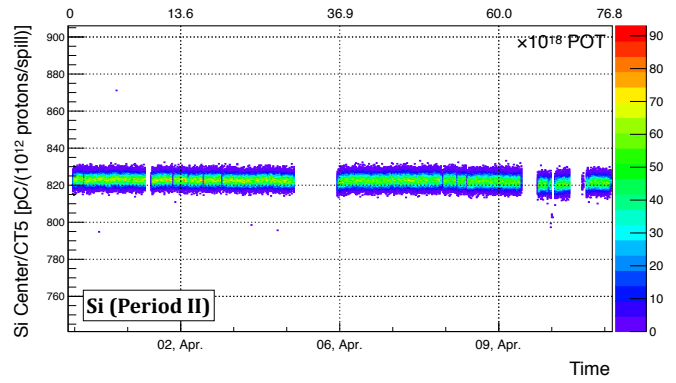
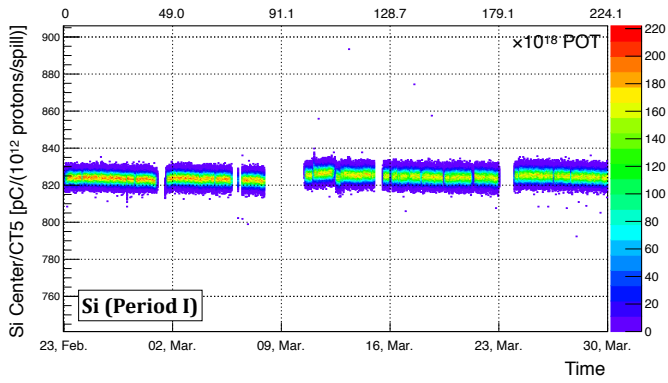


Figure 18: Signal yield of Si center channel as a function of time.

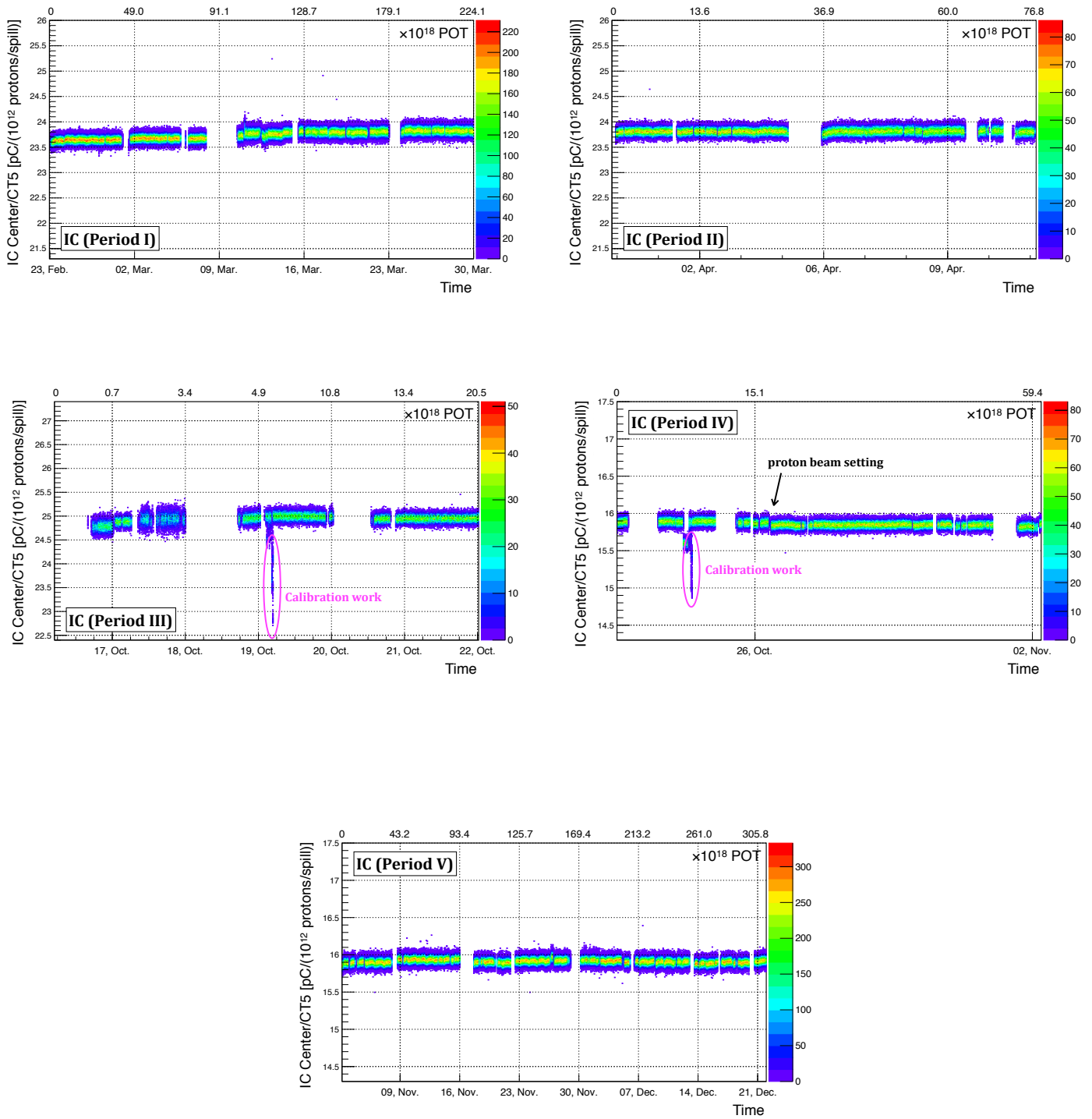


Figure 19: Signal yield of IC (Ar) center channel as a function of time. The yield jumps seen in Period III and IV, marked with magenta circles, are due to the calibration work where the entire IC system is moved (See Ref. [13] for the calibration method).

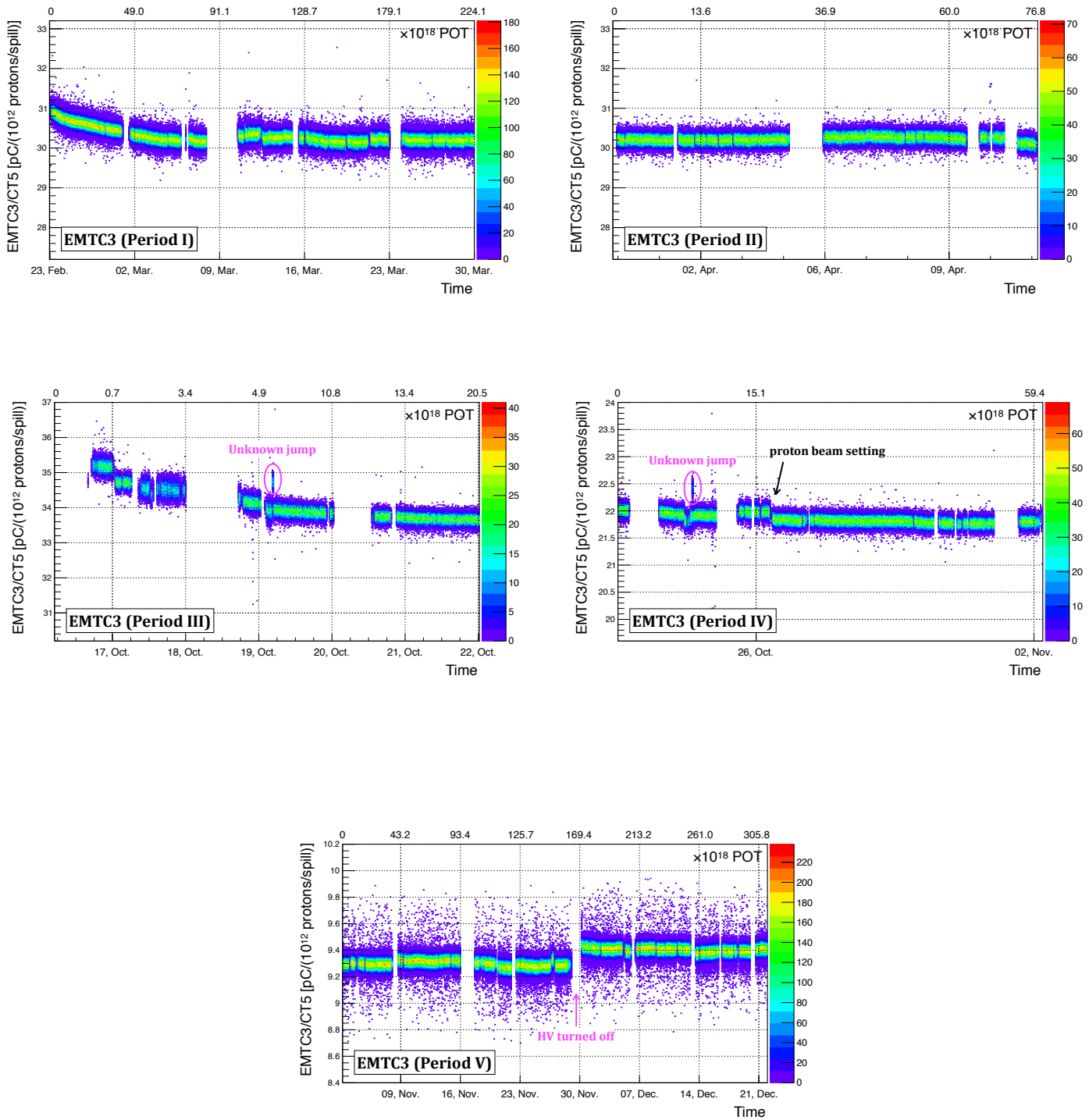


Figure 20: Signal yield of EMTC3 as a function of time. Two yield jumps are seen and seem to be synchronized with IC calibration work, although the cause is not fully understood. After a short HV off in Period V, the yield changed.

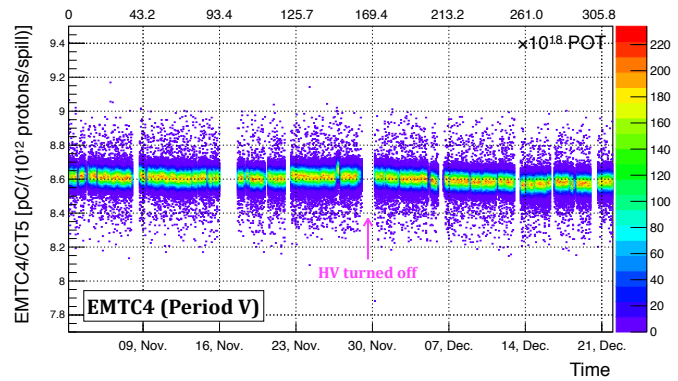
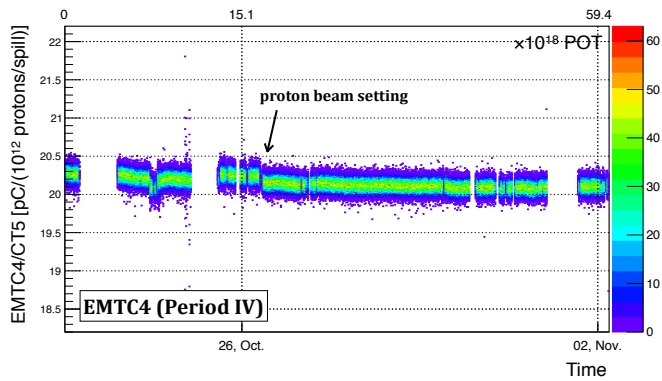
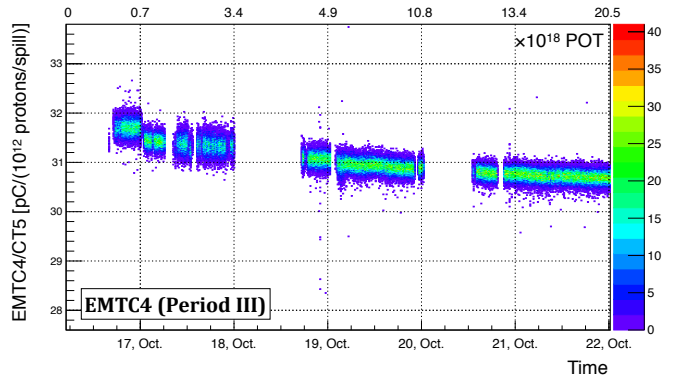
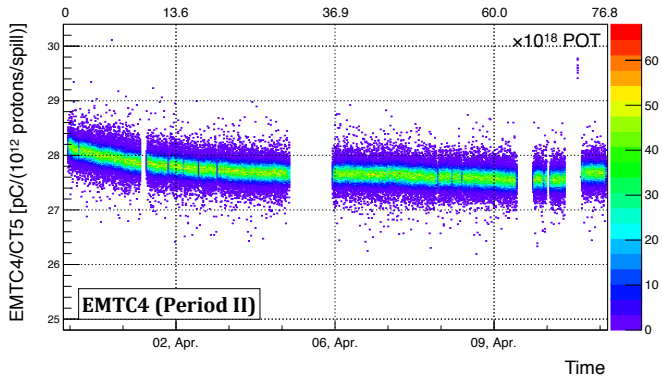


Figure 21: Signal yield of EMTC4 as a function of time. Other than the short periods just after the HV is turned on, C4 shows stable performance.

6. Conclusion

We are developing an electron-multiplier tube as a possible new muon monitor sensor for the T2K experiment. Two prototype detectors were prepared by modifying the resistances and capacitances of original divider circuits of Hamamatsu-made EMTs, and these sensors were installed in the muon monitor location. Various properties of EMTs were measured using the T2K muon beam. The EMTs' time response was found to be faster than the Si or IC sensors, which is of high importance in bunch-by-bunch monitoring. The spill-by-spill intensity resolution at the current T2K operation conditions is better than the 1% requirement. Linearity tests show that the EMT keeps its linearity within $\pm 1\%$ up to 460 kW at +250 kA horn current. The linearity may be further improved by improving the HV divider circuit configuration. The EMT signal yield gradually decreased during initial EMT operation, and then stabilized. One possible reason for this is the conditioning of the EMT dynode materials. This work is the first demonstration of the usage of EMTs for muon beam monitoring, and indicates a strong possibility of practical use in the future.

Acknowledgment

The authors are grateful to the J-PARC accelerator group for supplying a stable beam. This work was partially supported by MEXT KAKENHI Grant Number 25105002, 16H06288, 15J01714, and 17J06141.

References

- [1] J. B. M. Pattison, C. A. Ramm, and W. A. Venus, Neutrino Meeting, CERN, Geneva, Switzerland, 13-14 Jan., 1969, proceedings (1969).
- [2] S. Kopp et al., Nucl. Instr. Meth. Phys. Res. A 568, 503-519 (2006).
- [3] K. Abe et al., Nucl. Instr. Meth. Phys. Res. A 659, 106-135 (2011).
- [4] Y. Fukuda et al., Nucl. Instr. Meth. Phys. Res. A 501, 418-462 (2003).
- [5] K. Abe et al., Phys. Rev. Lett., 118, 151801 (2017).
- [6] K. Abe et al., Phys. Rev. D, 96, 092006 (2017).
- [7] A. K. Ichikawa, Nucl. Instr. Meth. Phys. Res. A 690, 27-33 (2012).
- [8] T. Sekiguchi et al., Nucl. Instr. Meth. Phys. Res. A 789, 57-80 (2015).
- [9] K. Abe et al., Nucl. Instr. Meth. Phys. Res. A 694, 211-223 (2012).
- [10] S. Bhadra et al., Nucl. Instr. Meth. Phys. Res. A 703, 45-58 (2013).
- [11] K. Matsuoka et al., Nucl. Instr. Meth. Phys. Res. A 624, 591-600 (2010).
- [12] T. Higuchi et al., Computing in High Energy and Nuclear Physics (2003).
- [13] K. Suzuki et al., Prog. Theor. Exp. Phys., 053C01 (2015).

- [14] K. Abe et al., arXiv:1607.08004 (2016).
- [15] Hamamatsu Photonics K. K., Photomultiplier Tubes Basic and Applications Third Edition (2007).
- [16] R. D. Winn and Y. Onel, Journal of Physics: Conference Series, 404, 012021 (2012).
- [17] K. Abe et al., Phys. Rev. D, 87, 012001 (2013).